JOURNAL OF GEOPHYSICAL RESEARCH, VOL. 106, NO. C9, PAGES 19,671–19,681, SEPTEMBER 15, 2001

Eastern North Pacific Subtropical Mode Water in a general circulation model: Formation mechanism and salinity effects

Shigeki Hosoda,[1,2] Shang-Ping Xie,[3] Kensuke Takeuchi,[1,4] and Masami Nonaka[3,5]

Abstract. The Eastern North Pacific Subtropical Mode Water (ESTMW) is a water mass of low potential vorticity (PV) and appears as a weak pycnostad or thermostad. Distinct from other subtropical mode waters, it forms in the absence of a deep winter mixed layer. The formation mechanism of this ESTMW is investigated using an ocean general circulation model that is forced by monthly climatological temperature, salinity, and wind stress at the sea surface. An equation based on the ventilated thermocline theory is used to diagnose the initial PV of a water mass right after its subduction. In this equation, three factors affect the initial PV: the spacing of density outcrop lines, the mixed layer depth gradient, and the vertical velocity at the bottom of mixed layer. Among them the wide spacing between outcrop lines is the most important for ESTMW's low PV instead of the deep mixed layer, which is most important for classical mode waters. It is found that weak gradients in both sea surface temperature and salinity in the direction of mixed layer flow are important for the low PV formation. A low-salinity tongue that extends southeastward off North America is responsible for the small surface density gradient in the eastern North Pacific and contributes to the formation of the ESTMW. An additional experiment forced with observed freshwater flux demonstrates that the southward advection of fresher water from the high latitude along the eastern boundary is the cause of this low-salinity tongue.

1. Introduction

In the subtropical gyres of the world oceans the existence of mode waters in the thermocline is well known. These mode waters appear as thermostads or pycnostads with weak vertical gradients in temperature and density. In the North Pacific, two major mode waters have been reported: the North Pacific Subtropical Mode Water (NPSTMW) [*Masuzawa*, 1969; *Suga and Hanawa*, 1995] on σ_θ = 25.4 in the western part of the basin and the North Pacific Central Mode Water (NPCMW) [*Nakamura*, 1996; *Suga et al*., 1997] on σ_θ = 26.2 in the central part. In the North Atlantic, 18°C water [*Worthington*, 1959; *McCartney*, 1982] exists in the south of the Gulf Stream. In the South Pacific, *Roemmich and Cornuelle* [1992] found a subtropical mode water off New Zealand. In volume census, mode waters occupy a large portion of the main thermocline, and their variabilities can have a significant effect on subsurface structures of the ocean. Indeed, recent idealized [*Inui et al*., 1999] and realistic [*Xie et al*., 2000] general circulation model (GCM) simulations suggest that the mode waters may undergo large zonal excursions as surface winds change, inducing large subsurface temperature anomalies.

The formation mechanism of these mode waters is not well understood, but the mixed layer distribution is considered to be important [*Huang and Qiu*, 1994; *Kubokawa*, 1999]. They often form near the extension of strong western boundary currents with intense wintertime cooling. Once formed, the mode waters are subducted into the main thermocline by the Ekman convergence and lateral induction and then transported south or southwestward, conserving potential vorticity (PV). The ventilated thermocline theory [*Luyten et al*., 1983] can explain this formation mechanism if the horizontal variation in mixed layer depth is considered [*Kubokawa*, 1999]. In a GCM forced by observed forcing, *Xie et al*. [2000] showed that the low PV around the gyre boundary was made at the cross point of the mixed layer depth front and density outcrop line, in support of the notion that the deep mixed layer is the key to the low-PV mode water. They also suggested that a diagnostic equation based on the thermocline model [e.g., *Williams*, 1991] can qualitatively explain the relation between the deep mixed layer and mode water, consistent with observations [e.g., *Bingham*, 1992]. Recently, *Hautala and Roemmich* [1998] found a new type of mode water in the eastern North Pacific by analyzing historical observations. This so-called Eastern North Pacific Subtropical Mode Water (ESTMW) is located around 25°–30°N, 140°W, with temperatures ranging from 16° to 22°C and σ_θ ranging from 24.0 to 25.4. They pointed out that the formation of this ESTMW is puzzling because the winter cooling is much less intense here than in the formation regions of other mode waters. *Xie et al*. [2000] suggest that the wide spacing of surface density isolines is important, while *Ladd and Thompson* [2000] emphasize the importance of winter mixed layer distribution. On the basis of one-dimensional mixed layer model calculations they suggest that the weak summer warming and a weak seasonal thermocline contribute to the deepening of local winter mixed layer.

[1]Institute of Low Temperature Science, Hokkaido University, Sapporo, Japan.
[2]Now at Japan Marine Science and Technology Center, Yokosuka, Japan.
[3]International Pacific Research Center, School of Ocean and Earth Science and Technology, University of Hawaii at Manoa, Honolulu, Hawaii, USA.
[4]Now at Frontier Observational Research System for Global Change, Yokosuka, Japan.
[5]Also at Frontier System for Global Change, Yokohama, Japan.

Copyright 2001 by the American Geophysical Union.

Paper number 2000JC000443.
0148-0227/01/2000JC000443$09.00

Table 1. Experiment Conditions

Experiment	Temperature Force	Salinity Force	Initial $T - S$
SD-RUN	restore	restore	climatology
ZT-RUN	restore to zonal mean	restore	zonal mean climatology
ZS-RUN	restore	restore to zonal mean	zonal mean climatology
SF-RUN	restore	zonal mean $P - E$ flux	zonal mean climatology

In this study we attempt to test these hypotheses and investigate the formation mechanisms for the ESTMW. We use the diagnostic equation of *Williams* [1991] and analyze an ocean GCM (OGCM) simulation to identify the major processes contributing to the ESTMW's low PV. The eastern North Pacific is a region where sea surface salinity (SSS) displays strong horizontal variations, which may affect the ESTMW and its PV. The relative importance of sea surface temperature (SST) and SSS distributions will be assessed diagnostically and by performing additional GCM experiments.

The rest of this paper is organized as follows. Section 2 describes the model, data, and experiments to be performed. Section 3 diagnoses the formation mechanism of the ESTMW by using a ventilated thermocline model. Section 4 examines the effects of salinity on the ESTMW. Section 5 offers some further discussions, and section 6 is a summary.

2. Model and Experiments

2.1. Model

We used the Geophysical Fluid Dynamics Laboratory modular ocean model, MOM 1.1 [*Pacanowski et al*., 1991]. It solves the primitive equations in spherical coordinates, under the Boussinesq, rigid lid, and hydrostatic approximations. It covers the North Pacific from 65°N to 15°S, with realistic coastal and bottom topography. The horizontal resolution is 1° by 1°, and there are 32 vertical levels with 10 m resolution near the sea surface. The horizontal and vertical eddy viscosities are constant at 1.0×10^8 and 5.0 $cm^2\ s^{-1}$, respectively. Temperature and salinity are mixed both isopycnally and diapycnally with background diffusivities of 2.0×10^7 and 0.3 $cm^2\ s^{-1}$, respectively [*Cox*, 1987]. The model employs the nonslip lateral boundary conditions and requires the fluxes of mass, temperature, and salinity to vanish at all boundaries except at the sea surface. We force the model with monthly mean climatological surface wind stress taken from the National Centers for Environmental Prediction (NCEP) reanalysis [*Kalnay et al*., 1996] for 1958–1997. SST and SSS are restored toward the *World Ocean Atlas 1994* (*WOA94*) monthly climatology data [*Levitus and Boyer*, 1994; *Levitus et al*., 1994] with a time constant of 14 days [*Haney*, 1971]. Near the poleward boundaries of the OGCM, temperature and salinity are restored to the *WOA94* monthly climatology data at all vertical levels. The restoring time constant is 2 days at the north and south walls and decreases exponentially to infinity toward the interior within 8° off each wall. The OGCM is integrated for 30 years from the resting state with the *WOA94* monthly mean temperature and salinity.

In addition to this standard (SD) control run, three sensitivity experiments (Table 1) are performed. They will be described in more detail in section 4.2.

2.2. Comparison With Observations

First, we compare the OGCM simulation (SD-RUN) with observations (*WOA94*, Levitus monthly climatology). We neglect relative vorticity contribution to PV, which is generally small except near strong currents, namely,

$$q = -\frac{f}{\rho_0} \cdot \frac{\partial \rho}{\partial z}, \tag{1}$$

where q is PV, f is the Coriolis parameter, z is the vertical coordinate, ρ is the seawater density, and ρ_0 is its reference value.

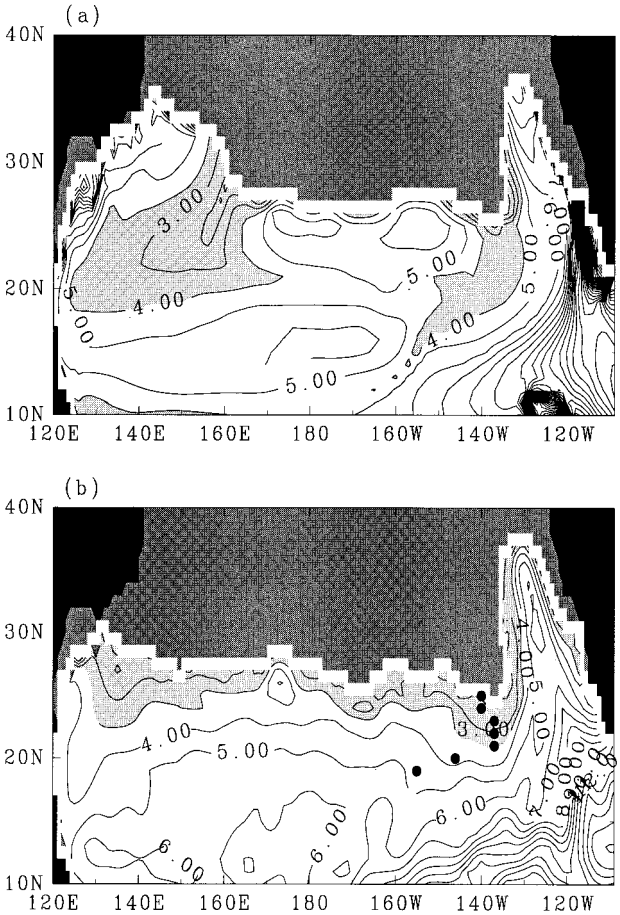

Figure 1. (a) March PV ($\times 10^{-10}$ $m^{-1}\ s^{-1}$) on the σ_θ = 24.75 surface in the SD-RUN. The low-PV regions ($<4.0 \times 10^{-10}$ $m^{-1}\ s^{-1}$) are shaded. Dark shading is the outcrop area. (b) Same as Figure 1a except for the observed climatology on the σ_θ = 24.9 surface (shade $< 3.0 \times 10^{-10}$ $m^{-1}\ s^{-1}$). Solid circles denote the PV minima at each latitude around the eastern North Pacific.

The model ESTMW forms around 140°W, 25°N, at nearly the same place as in observations (Figure 1). In the model the PV minimum of the ESTMW is advected in a southwestward direction after subduction, while in observations, its signature is hard to trace away from its formation and presumably is obscured by spatial smoothing in preparing the gridded climatology. Figure 2 shows the density and PV distributions in March along 24°N. A distinctive PV minimum is found below the winter mixed layer (short-dashed line) in both the OGCM and Levitus climatology fields around 140°W. The density range for this PV minimum is 24.2–25.0 σ_θ in the OGCM and 24.5–25.0 σ_θ in observations [*Hautala and Roemmich*, 1998]. Quantitatively, the simulated PV is too large compared with observations. The model thermocline is too shallow in the eastern Pacific, and as a result, the PV minimum penetrates too shallow a depth in comparison with observations.

Despite these quantitative differences the model simulates the ESTMW at the right geographic location and on the right density surfaces. Encouraged by these qualitative agreements with observations, we feel that the OGCM captures the key processes involved in the ESTMW formation and will proceed to discuss them in the context of this particular OGCM.

3. Formation Mechanism

To examine the formation mechanism, we use the ventilated thermocline model with the mixed layer in the subtropical gyre

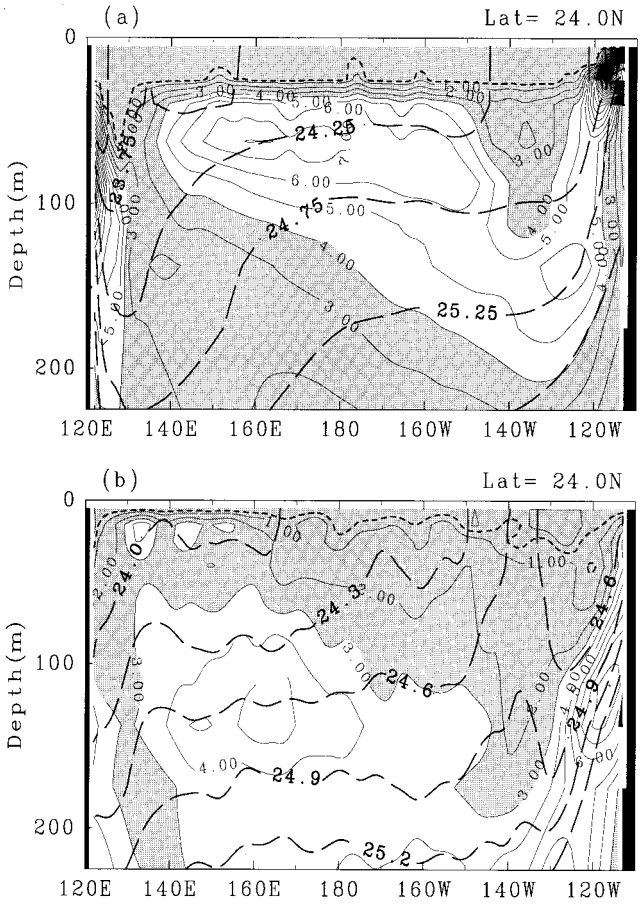

Figure 2. (a) March PV (solid line; shade $< 4.0 \times 10^{-10}$ m^{-1} s^{-1}) at 24.0°N in the SD-RUN. The short-dashed line denotes the bottom of the mixed layer. (b) Same as Figure 2a except for the observed climatology (shade $< 3.0 \times 10^{-10}$ m^{-1} s^{-1}). Thick long-dashed contours are for σ_θ.

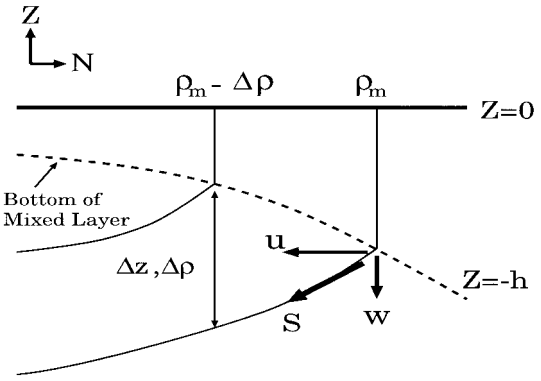

Figure 3. Schematics of the thermocline model on a meridional section. The winter mixed layer is above the dashed line ($Z = -h$). The arrows below the mixed layer denote the horizontal velocity (lateral induction) u, subduction rate S, and vertical velocity w on density (ρ_m) surface, respectively. Δz and $\Delta\rho$ are the depth and density differences between the subducted parcel and the overlying mixed layer.

[e.g., *Williams*, 1991; *Kubokawa*, 1999]. The schematic north-south section of the thermocline is shown in Figure 3. The PV at the bottom of the mixed layer, q_m, can be calculated in the model by recasting (1),

$$q_m = -\frac{f}{\rho_0}\frac{\partial \rho}{\partial z} = -\frac{f\Delta\rho/\Delta t}{\rho_0 \Delta z/\Delta t} = -\frac{f\Delta\rho/\Delta t}{\rho_0 S}, \tag{2}$$

where $\Delta\rho/\Delta t$ and $\Delta z/\Delta t$ are the rates of increase in the difference of density and depth between subducted parcel and overlying mixed layer, respectively. Further, $\Delta\rho/\Delta t$ is rewritten as

$$\frac{\Delta\rho}{\Delta t} = \frac{\partial \rho_m}{\partial t} + u\nabla\rho_m, \tag{3}$$

and S is the subduction rate,

$$S = \frac{\Delta z}{\Delta t} = -\left(w + \frac{\partial h}{\partial t} + u\nabla h\right), \tag{4}$$

where h is the depth of the mixed layer, w is the vertical velocity, and u is the horizontal current velocity at the bottom of the mixed layer. As we are only interested in the climatological steady state, we set $\partial\rho_m/\partial t = 0$ and $\partial h/\partial t = 0$. By doing so we need to use the late winter (March) distributions for ρ and h. *Stommel* [1979] shows that in the presence of seasonal cycle, only the fluid leaving the deep winter mixed layer irreversibly enters the main thermocline, the so-called the "Stommel demon."

Under this steady state Stommel demon assumption, (2) finally becomes

$$q_m = \frac{f}{\rho_0}\frac{u\nabla\rho_m}{(w + u\nabla h)}, \tag{5}$$

where all the variables are for the late winter (March). According to (5) the value of q_m is determined by three factors: the product of the lateral velocity and the mixed layer depth gradient ($u\nabla h$), the vertical velocity (w), and the product of the horizontal velocity and the horizontal density gradient ($u\nabla\rho_m$) at the bottom of the mixed layer. We briefly consider how each of these three factors works to produce low-PV water. The $u\nabla h$ term in the denominator becomes large if the

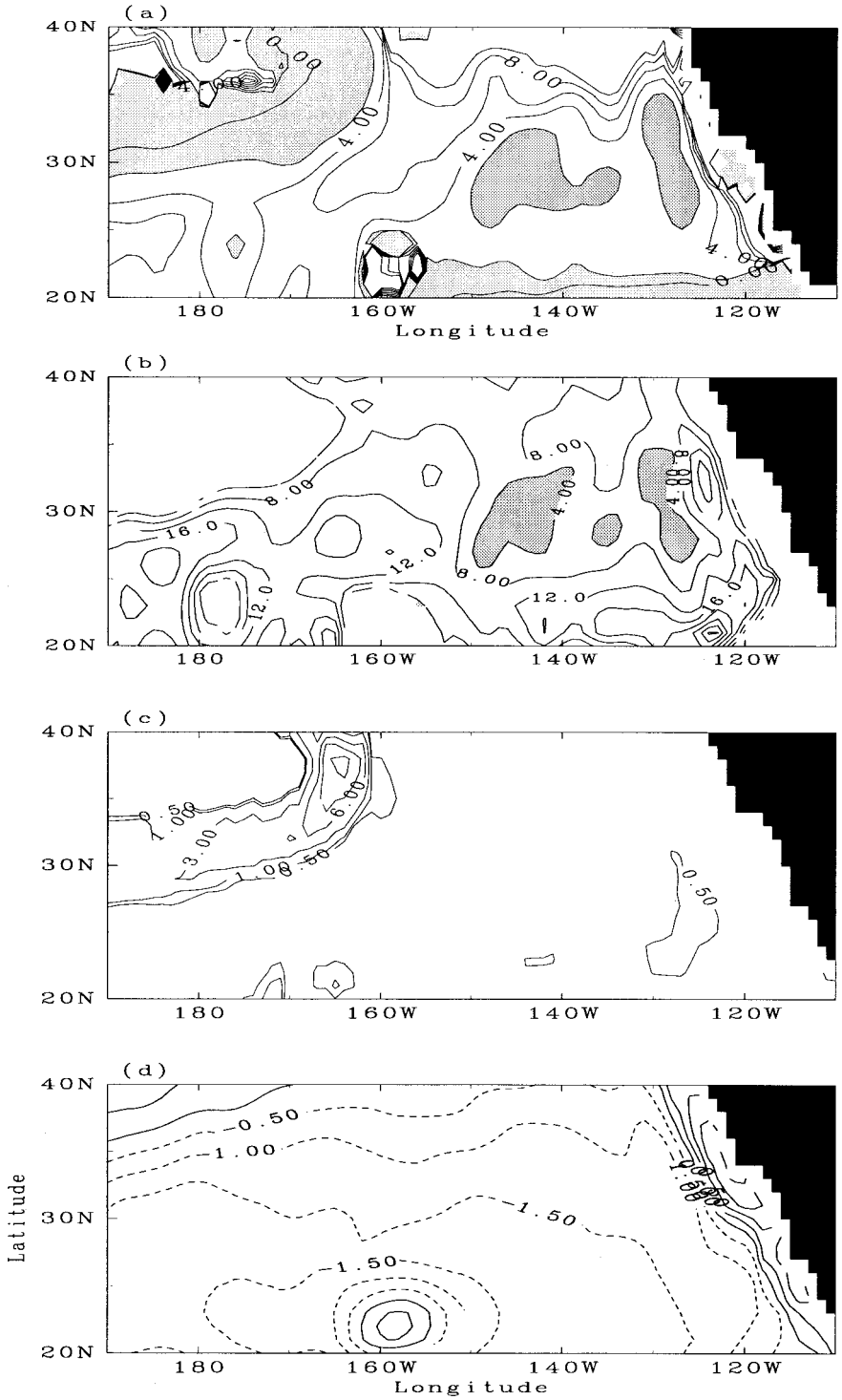

Figure 4. (a) PV at the subduction point (q_m in 10^{-10} m^{-1} s^{-1}) diagnosed from (5) in the SD-RUN (solid line). Contour intervals are 2.0×10^{-10} m^{-1} s^{-1} with low q_m ($< 2.0 \times 10^{-10}$ m^{-1} s^{-1}) shaded. Contours of values $>10.0 \times 10^{-10}$ m^{-1} s^{-1} are omitted. (b) Density advection effect $u\nabla\rho_m$ (shade $<4.0 \times 10^{-7}$ kg m^{-2} s^{-1} in the eastern North Pacific). Negative contours are omitted. (c) Lateral induction $u\nabla h \times 10^{-6}$ m s^{-1} with the 3.0×10^{-6} contour intervals. The contours with 0.5×10^{-6} intervals are also plotted ($<1.0 \times 10^{-6}$ m s^{-1}). (d) Upward vertical velocity w ($\times 10^{-6}$ m s^{-1}) at the bottom of mixed layer in (5).

gradient of the mixed layer depth is large and normal to horizontal current direction or if the horizontal current velocity is strong. In this case a large volume of vertically homogeneous water is subducted into the thermocline. The vertical velocity w acts simply to push water down into thermocline. The numerator, $u\nabla\rho_m$, is small if the horizontal density gradient normal to the horizontal current velocity is weak.

Figure 4a shows the distribution of q_m calculated from (5). There are two groups of low-q_m regions (shaded) in the northwestern and the eastern North Pacific, respectively. The former

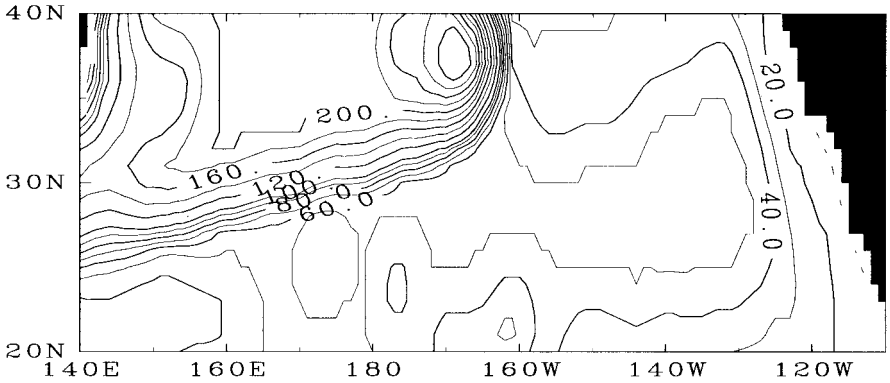

Figure 5. Mixed layer distribution (meters) with 10 m intervals (20 m for $h > 100$ m).

corresponds to the formation of the NPCMW and NPSTMW, whereas the latter corresponds to the ESTMW. This paper focuses on the latter low-q_m region in 150°–125°W, 25–33°N.

To understand the cause of the low q_m, we examine each of the three factors in (5); $u\nabla\rho_m$ (Figure 4b), $u\nabla h$ (Figure 4c), and w (Figure 4d). The low q_m in the northwestern Pacific is due to the lateral induction ($u\nabla h$) across a strong mixed layer depth front (Figure 5). Neither the lateral induction nor vertical velocity w shows significant zonal variations in ESTMW's formation region. There is a weak minimum in lateral induction around 130°W, 25°N due to a weak mixed layer depth front there. This minimum in lateral induction rate is too weak to account for the minimum we see in q_m. We note, however, that the observed mixed layer depth shows a somewhat stronger maximum in the mixed layer depth around ESTMW's formation region, giving rise to a local maximum in subduction rate [*Huang and Qiu*, 1994].

By contrast, the distribution of the density advection effect $u\nabla\rho_m$ bears a strong resemblance to q_m in the eastern North Pacific, indicating that it is the most important for the ESTMW. The surface density gradient is many times smaller in ESTMW's formation region than west of 150°W (Figure 6a). Intuitively, the total volume of subducted water between two neighboring outcrop lines increases with the spacing between them even if the subduction rate is constant in space. The ESTMW forms because of the wide spacing of surface density isolines in the eastern North Pacific.

As in most of the subtropical gyre, the mixed layer depth in the eastern North Pacific reaches a seasonal maximum in March. Using a one-dimensional mixed layer model, *Ladd and Thompson* [2000] suggest that the local maximum in winter mixed layer depth in the eastern North Pacific is due to weak seasonal warming in summer and is important for the ESTMW. Our analysis here and in the following indicates that the formation of the ESTMW is nonlocal, for which the horizontal gradient of surface density, both its magnitude and direction relative to current velocity, is also important.

Once it is formed, the ESTMW enters the thermocline and is advected south and southwestward along the isopycnals (Figure 1a). The PV minimum gradually diffuses away and becomes nearly invisible when it reaches the southern flank of the subtropical gyre.

4. Relative Importance of Temperature and Salinity

Figure 6 displays the March sea surface density, SST, and SSS in the SD-RUN. There are tongues of low temperature and salinity off North America directed to the southeast. They are partly density-compensated between each other and responsible for the weak density gradient that is important for the ESTMW formation. Figure 7 shows vertical gradients of temperature and salinity, $\partial T/\partial z$ and $\partial S/\partial z$, along 24°N with low q shaded. Within the ESTMW (140°W, 50–100 m), $\partial T/\partial z$ is generally small, in support of *Hautala and Roemmich*'s [1998] temperature-based PV analysis. Compared to the upper part of the ESTMW, $\partial T/\partial z$ is relatively high in the lower part. The PV remains low in the lower ESTMW because large $\partial S/\partial z$ offsets the increasing $\partial T/\partial z$. The salinity gradient is positive, which by itself is an unstable stratification. Thus, along with temperature the salinity distribution appears also important especially in the lower part of the ESTMW. In this section we examine the relative importance of temperature and salinity for ESTMW formation.

4.1. Diagnosis

We decompose a density change into temperature and salinity components,

$$\Delta\rho = \frac{\partial\rho}{\partial T}\Delta T + \frac{\partial\rho}{\partial S}\Delta S \equiv \alpha\Delta T + \beta\Delta S. \tag{6}$$

Using this linear equation, we can decompose q_m into temperature and salinity contributions, q_m^T and q_m^S, respectively,

$$q_m = Ku(\alpha\nabla T) + Ku(\beta\nabla S) = q_m^T + q_m^S, \tag{7}$$

where

$$K = -\frac{f}{\rho_0}\frac{1}{w + u\nabla h}. \tag{8}$$

Here we use $\alpha = -0.000255$ and $\beta = 0.000764$ for a reference state of 18°C and 34.5 psu [cf. *Gill*, 1982]. Figure 8 displays the distributions of q_m^T and q_m^S. In the eastern North Pacific, q_m^T is small, with values below 4.0×10^{-10} m^{-1} s^{-1} over most of the low-q_m regions. Thus the SST distribution is instrumental in low-q_m formation. On the other hand, large negative q_m^S values are found on the western and eastern sides of the broad low-q_m region, indicative of the salinity effect to reduce q_m. Between the two shaded low q_m centers, however, q_m^S shows small positive values, suggesting that the salinity does not always act to reduce PV. Its effect varies in different parts of ESTMW formation region.

To show the relative contributions by T and S more clearly, we plot the zonal distributions of q_m, q_m^T, and q_m^S averaged in the latitudinal band of the low q_m (26° and 32°N; Figure 9).

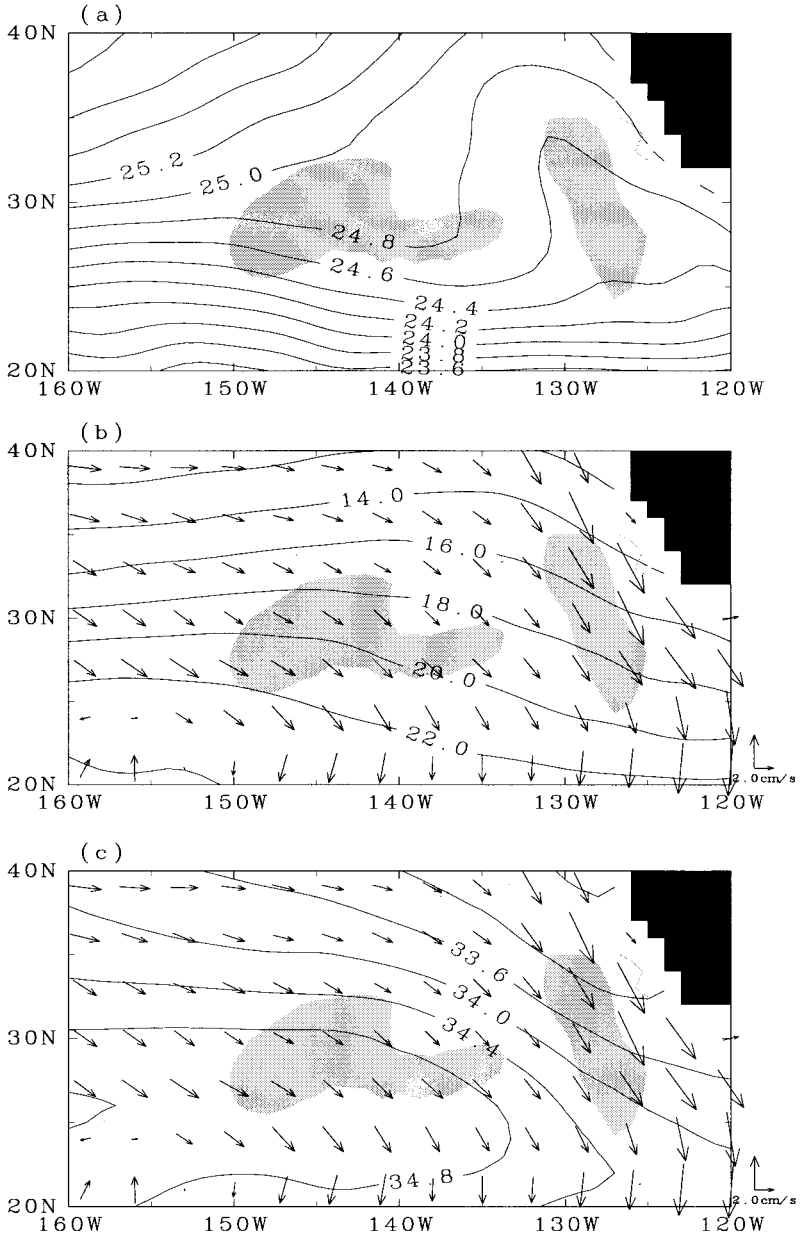

Figure 6. March (a) surface density (σ_θ), (b) SST (°C) and (c) SSS (psu), along with current vectors at the bottom of the mixed layer in the SD-RUN. Low q_m areas are shaded.

Values of q_m^T are generally larger than q_m, an effect of the generally negative q_m^S. While q_m^T is responsible for large-scale distribution of the low q_m, q_m^S is also important, especially in the eastern (east of 130°W) and western (west of 145°W) edges of the low q_m. So, this low-q_m region can be divided into three subregions: one mainly due to low q_m^T and the eastern and western parts of the low q_m, where the q_m^S contribution is crucial.

To understand further the distributions of q_m^T and q_m^S, we examine the temperature and salinity distributions in relation to current velocity at the bottom of mixed layer (Figures 6b and 6c). The low q_m (shaded) is mainly due to weak SST gradient and, to a less degree, to weak current velocity. Because of the negative β, strong salinity advection helps form low PV. Such salinity advection is strongest in the eastern low-q_m region and is also significant in the western one. In the central region the salinity advection is small despite a large salinity gradient.

Equation (7) can be recast as

$$q_m^T + q_m^S = KU\{\alpha G_T \sin \varphi_T + \beta \cdot G_S \sin \varphi_S\}, \qquad (9)$$

where U is the current speed, G_T (G_S) is the magnitude of horizontal temperature (salinity) gradient, and φ_T (φ_S) is the angle between the current direction and the temperature (salinity) isolines (Figure 10). Because the ocean current flows in a general southeast direction in the eastern subtropical gyre, SST isolines that slant southeastward (a small φ_T as in Figure 10) favor the formation of low-PV water by reducing the SST advection. Figures 11a and 11b show the zonal distributions of q_m^T (q_m^S), G_T (G_S), sin φ_T (sin φ_S), and U averaged between 26° and 32°N. As we are only concerned with their relative

importance and for clarity, we normalize these variables with their values at 125°W. All three variables $[U]$, $[G_T]$, and [sin φ_T] contribute to the $[q_m^T]$ minimum at 145°–135°W. Among them, $[G_T]$ varies by a factor of 2 at 155°–140°W and appears to be the most important. (The rapid increase of $[q_m^T]$ around 125°W is, however, associated with that in $[U]$ and [sin φ_T].) The zonal distribution of $[q_m^S]$, on the other hand, largely follows that of [sin φ_S]. The advection of salinity acts generally to lower $[q_m]$ values except in a small region centered at 135°W where $[G_T]$ actually is at its maximum.

In this method, current speed is also included in the denominator. This influence, however, is weak because of small $u\nabla h$ (Figure 4c) and weak mixed layer front (Figure 5) in the eastern North Pacific.

4.2. Sensitivity Experiments

Zonal variations in SST and SSS are the cause of ESTMW's low PV, unlike the western mode waters that result from strong gradients in the mixed layer depth distribution. Here we conduct two sensitivity experiments to see the changes in the ESTMW when zonal variations in either SST or SSS are removed. In the ZT- (ZS-) RUN we restore SST (SSS) to the zonal mean values while using the observed climatology for the other density component. To reduce the initial shock, we use the zonal mean temperature (salinity) field in the SD-RUN as the initial conditions for the ZT- (ZS-) RUN. In both experiments the model is integrated for 30 years.

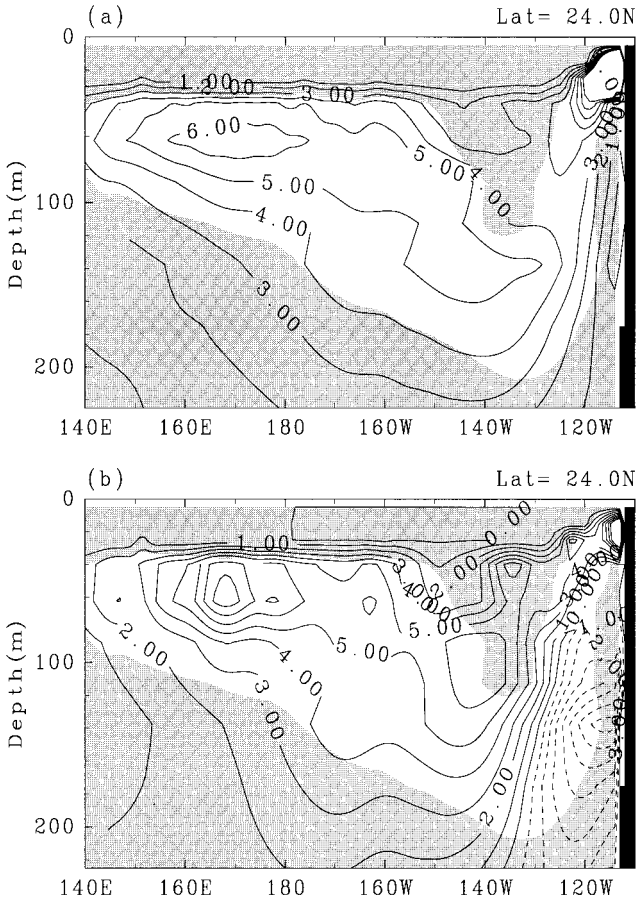

Figure 7. Zonal sections of (a) $\partial T/\partial z$ (°C m^{-1} × 100) and (b) $\partial S/\partial z$ (psu m^{-1} × 1000) in the SD-RUN. Regions of PV < 1.0×10^{-10} m^{-1} s^{-1} are shaded.

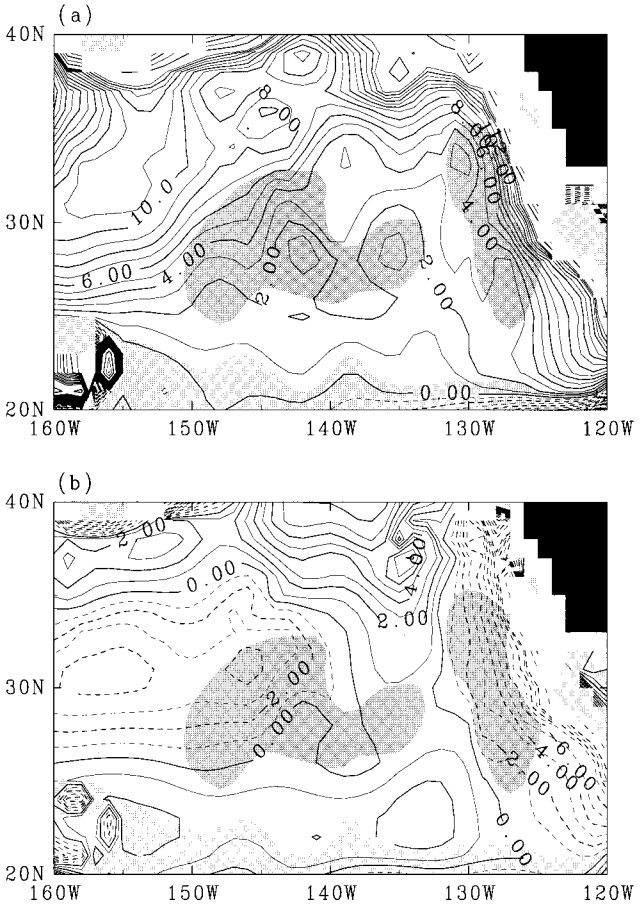

Figure 8. (a) Distribution of q_m^T ($\times 10^{-10}$ m^{-1} s^{-1}) in the SD-RUN. Contour intervals are 1.0×10^{-10} m^{-1} s^{-1} for $q_m^T <$ 15.0×10^{-10} m^{-1} s^{-1} and 5.0×10^{-10} m^{-1} s^{-1} for $q_m^T <$ 15.0×10^{-10} m^{-1} s^{-1}. Low-q_m values are shaded (see Figure 4a). (b) Same as Figure 8a except for q_m^S with contour intervals of 1.0×10^{-10} m^{-1} s^{-1} for $q_m^S > -10.0 \times 10^{-10}$ m^{-1} s^{-1} and 5.0×10^{-10} m^{-1} s^{-1} for $q_m^S < -10.0 \times 10^{-10}$ m^{-1} s^{-1}.

Figure 12 shows the zonal sections of PV along with σ_θ and mixed layer depth in these experiments. In the ZT-RUN (Figure 12a) the low-PV region does not exist (compare with Figure 2a). In the ZS-RUN (Figure 12b), on the other hand, a weak PV minimum is found below the winter mixed layer near

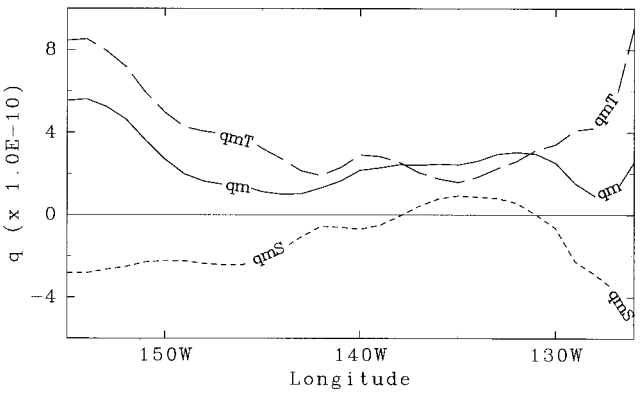

Figure 9. Zonal distributions of q_m (solid line), q_m^T (long-dashed line), and q_m^S (dashed line) averaged between 26° and 32°N in the SD-RUN.

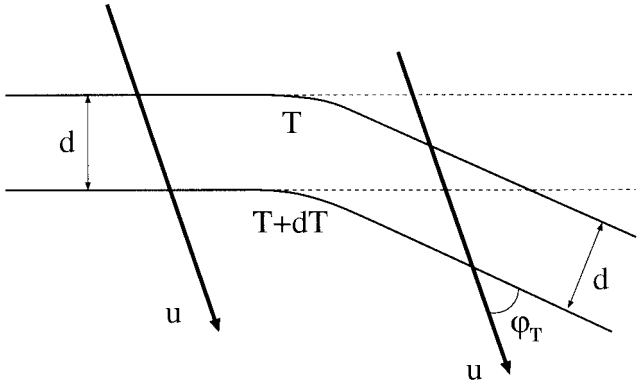

Figure 10. Schematic for the effect of slanting SST isolines, where d is the width between SST isolines and φ_T is the angle between a SST isoline and the current velocity at the bottom of the winter mixed layer.

the eastern boundary, but its location is shifted 15° eastward compared to the SD-RUN. The σ_θ fields in both runs look rather different from that in Figure 2a. These results show that zonal variations in both temperature and salinity are necessary for a realistic simulation of the ESTMW with the right strength and location.

The restoring boundary condition for SSS is physically unrealistic and unsuitable for studying the formation mechanism for the observed SSS distribution. The SF-RUN uses the freshwater flux boundary condition for salinity to understand better the SSS distribution in the eastern North Pacific. Monthly mean freshwater flux is calculated from the Global Positioning Climatology Project precipitation [*Huffman et al.*, 1995], the NCEP reanalysis runoff, and evaporation. The annual mean precipitation minus evaporation ($P - E$) distribution in the North Pacific is nearly zonally uniform, with excessive precipitation in middle and high latitudes along 40°N (Figure 13, shaded) and excessive evaporation in the subtropics. Low evaporation due to low SSTs and high precipitation in the atmospheric storm track both contribute to the positive freshwater flux north of 33°N. We further zonally average the freshwater flux before applying it to the model to illustrate the ocean advective effect.

Figure 14a shows the surface salinity distribution under this $P - E$ flux boundary condition. Though the absolute values are too high, the gross distribution pattern of SSS resembles

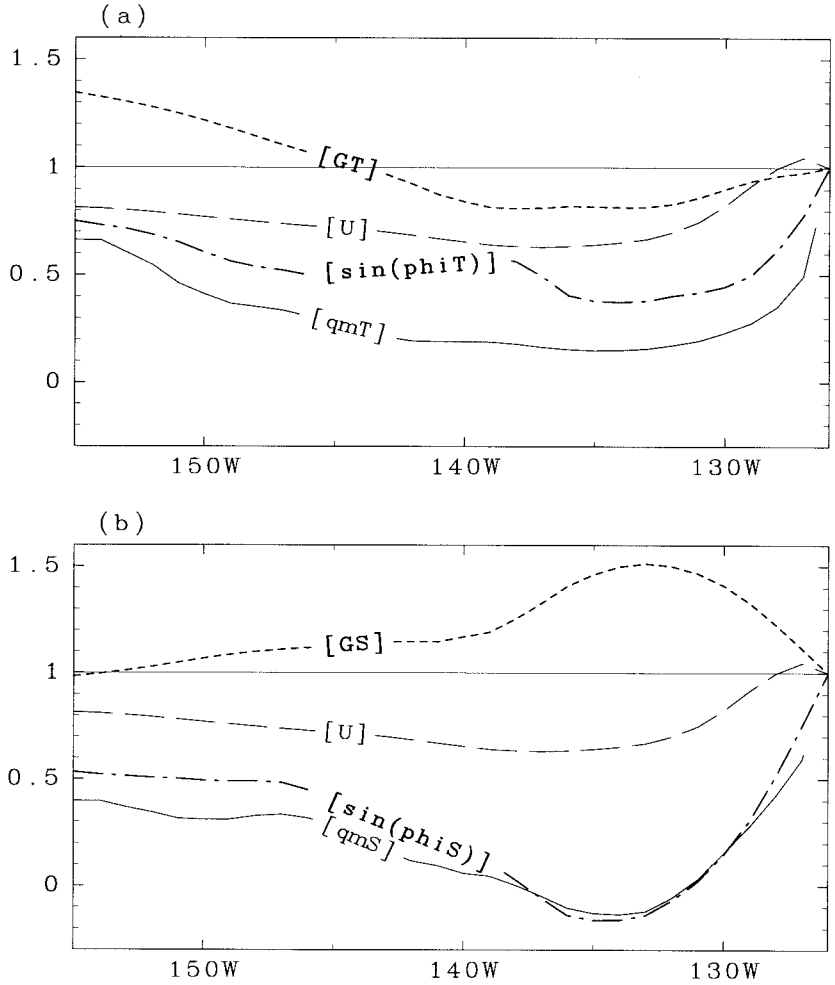

Figure 11. (a) Normalized q_m^T ([qmT]; solid line), $|\nabla T|$ ([G_T]; dashed line), current magnitude ([U]; long-dashed line), and sin φ_T ([sin phiT]; dot-dashed line) distributions averaged between 26° and 32°N in the SD-RUN. (b) Same as Figure 11a except for q_m^S ([qmS]; solid line), $|\nabla S|$ ([G_S]; dashed line), current magnitude ([U]; long-dashed line), and sin φ_S ([sin phiS]; dot-dashed line). The normalization is performed against the value at 125°W.

that in the SD-RUN. In particular, there is a low-salinity tongue off the east coast of North America apparently due to the advection of less saline water from the north by relatively strong eastern boundary current (see Figure 13). Figure 14b shows the zonal section of q at 24°N in March in the SF-RUN. The low-PV water is reproduced, though shifted slightly eastward compared to Figure 2a in the SD-RUN. The PV minimum is weaker than in the SD-RUN but stronger than in the ZS-RUN without zonal variations in SSS. It follows that the low-salinity tongue off North America results from the strong advection by the eastern boundary current and that it makes an important contribution to the formation of low-PV water in the eastern North Pacific.

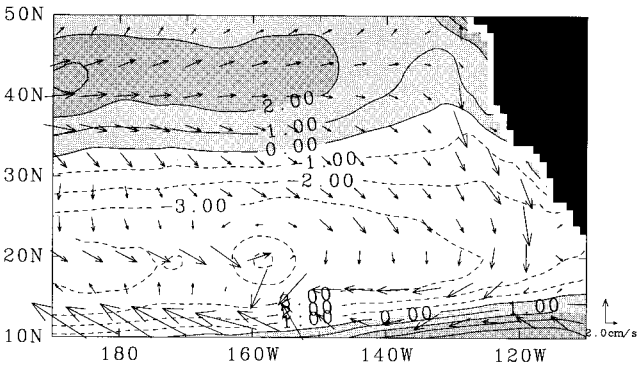

Figure 13. Annual mean $P - E$ flux (contours in mm d^{-1}; shade > 0) and surface current velocity vectors (cm s^{-1}) in the eastern North Pacific.

5. Discussion

We now turn our attention to the cause of zonal variations in SST. North of 25°N, SST isolines show a ridge that extends northeastward from 155°W, 25°N to 130°W, 40°N (Figure 15a). At the same time, there is a SST trough to the south that extends southwestward. This SST ridge and trough pair is responsible for the weak SST gradient and the southeast tilt of its isolines, two features key to the ESTMW formation (Figure 11a). To the west of the SST ridge, there are strong southwesterly winds, whereas there are strong northeasterlies over the SST trough. These winds are apparently part of an anticyclonic circulation off the California coast. The strong southwesterlies blow across strong meridional SST gradients, advecting warm and moist air northward. Indeed, in the observed climatology, there is a maximum in relative humidity slightly to the west of the SST ridge (Figure 15b), indicative of this meridional advective mechanism. The warm and moist air advected from the south suppresses the sensible and latent heat flux from the ocean, thereby causing an eastward increase in SST over this region of prevailing southwesterlies. The general eastward decreasing trend of westerly wind speed between 170° and 130°W

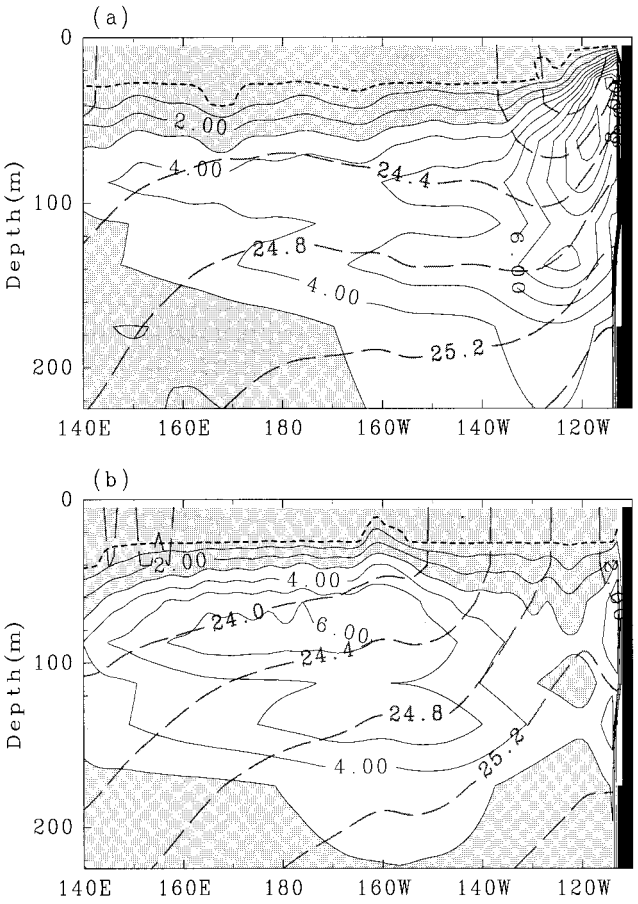

Figure 12. PV (solid contours in 10^{-10} m^{-1} s^{-1}; shade $< 3.0 \times 10^{-10}$ m^{-1} s^{-1}) and σ_θ (dashed contours) at 24°N in (a) the ZT- and (b) the ZS-RUN.

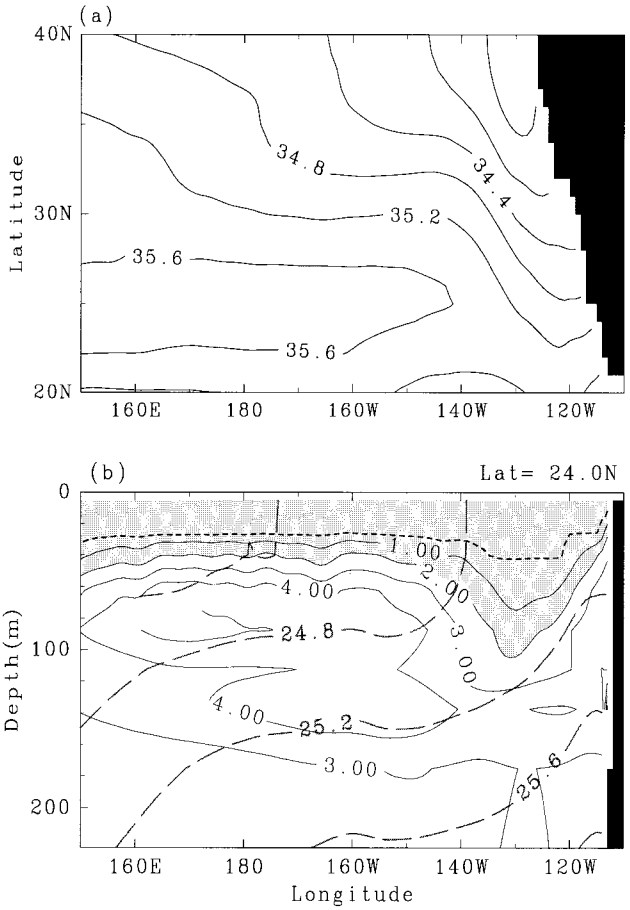

Figure 14. (a) March surface salinity and (b) q (solid contours; shade $< 10^{-10}$ m^{-1} s^{-1}) and σ_θ (dashed) in the SF-RUN. Short-dashed line is the bottom of the mixed layer.

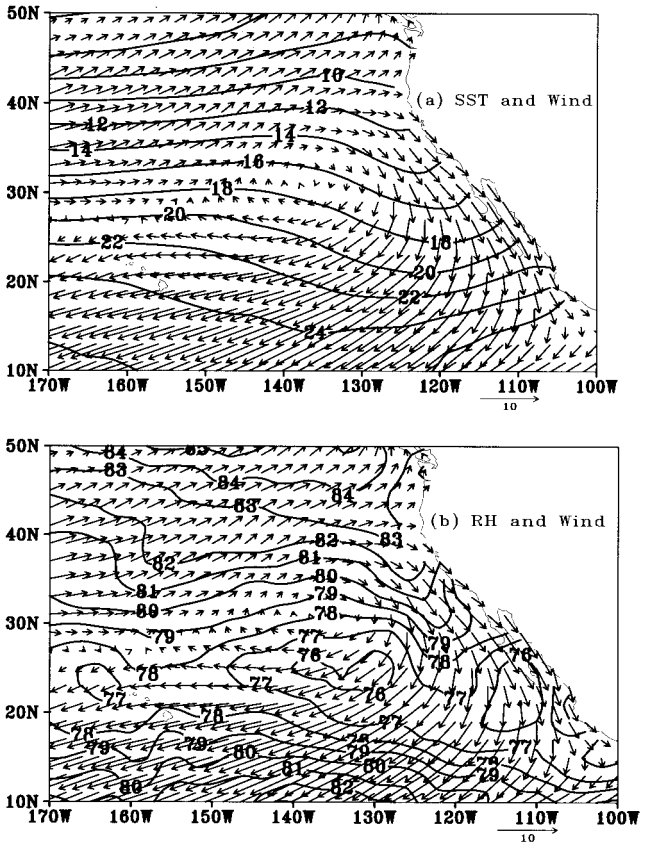

Figure 15. (a) SST (°C) and (b) relative humidity (%) in February along with surface wind velocity (m s^{-1}). Based on the Comprehensive Ocean Atmosphere Data Set.

also appears to contribute to the eastward increase in SST, by reducing the southward Ekman advection. The SST decrease east of the SST ridge is apparently due to the coastal upwelling and influence of continent. The cooling near North America causes the SST isolines to slant toward the southeast, an orientation in favor of the ESTMW formation (Figure 6b).

Figure 16 shows the sea level pressure and 500 hPa geopotential height in February. The pronounced ridge at 500 hPa on the west coast of North America is part of planetary-scale

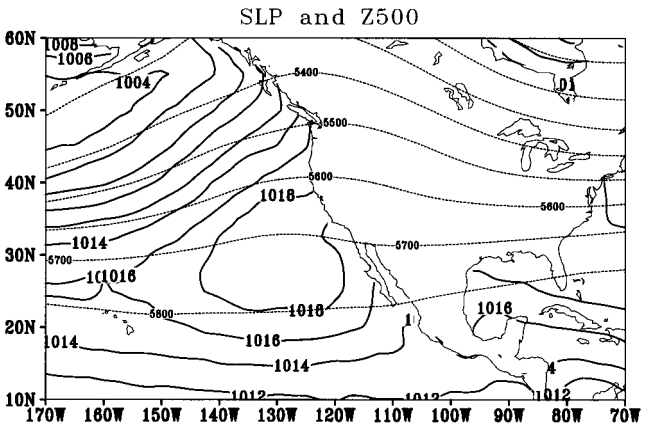

Figure 16. SLP (solid in hPa) and 500 hPa geopotential height (dotted in m) in February based on the NCEP reanalysis.

stationary waves induced by zonal variations in tropical SST and by orographic features such as the Tibetan Plateau [e.g., *Held*, 1983; *Inatsu et al*., 2000]. These stationary waves have deep barotropic structure, and the high sea level pressure (SLP) center off California appears to be a surface signature of this upper level ridge. This anticyclonic circulation helps form the ESTWM to the west of its center by two means. First, it advects air and moisture so as to reduce the SST gradient. Second, it causes strong cooling off North America, bending the SST isolines southeastward.

The NPSTMW and NPCMW form in a deep winter mixed layer and are both a pycnostad and a thermostad. By contrast, the ESTMW forms in a region of much less intense winter cooling, and its deeper part shows relatively large vertical temperature gradients that are compensated by salinity gradients. Forming in a region of large horizontal salinity gradient, the ESTMW is best captured by analyzing density structure. Using only temperature measurements, which are more abundant than salinity ones, may underestimate the vertical extent of the ESTMW.

6. Summary

We have investigated the formation mechanism of the ESTMW in the North Pacific using an OGCM. A diagnostic equation based on the ventilated thermocline theory is used to identify the major mechanism for low PV of the mode water. The model PV (q_m) is determined by three effects: Ekman pumping w, lateral induction ($u\nabla h$) and, horizontal density advection ($u\nabla\rho_m$). Our diagnosis indicates that the last effect is most important for the low-q_m formation in the eastern North Pacific. We conclude that the wide spacing of the density outcrop lines (or weak surface density gradient) is responsible for the ESTMW. Thus the formation mechanism for the ESTMW is different from that for the other western mode waters, which require a strong mixed layer front [*Kubokawa*, 1999; *Xie et al*., 2000]. The effects of surface density variations have been a focus of recent studies on decadal variations that show that these effects extend far away from the buoyancy forcing region in the subtropical thermocline [e.g., *Nonaka and Xie*, 2000; *Huang and Pedlosky*, 2000].

In the eastern North Pacific, large-salinity gradients exist that strongly affect the density distribution at both the surface and depth. Decomposing the surface density gradient into temperature and salinity gradients, we show that the weak horizontal temperature gradient is more important, but salinity also contributes significantly to low PV. This is further demonstrated in sensitivity experiments where either SST or SSS is restored back to the zonal mean field. In either the ZT- or ZS-RUN the ESTMW is not well simulated in terms of its strength and longitude. In an experiment where the observed $P - E$ flux is applied, on the other hand, the model qualitatively reproduces the observed surface salinity field and the ESTMW. This demonstrates that the strong advection by the eastern boundary current is the cause of the low-salinity tongue off North America, which in turn helps form low-PV water in the eastern North Pacific.

Among the three North Pacific subtropical mode waters, the present OGCM simulates the ESTMW most realistically because its low PV is determined largely by the surface density distribution, which largely follows the prescribed equilibrium distributions given weak currents (<2 cm s^{-1}) in the ESTMW's formation region. By contrast, it remains a challenge to

simulate realistically the NPSTMW and NPCMW that form in regions of strong currents (>10 cm s^{-1}). Mesoscale eddies can strongly affect the ocean currents and, for example, appear responsible for the double-jet structure in the Kuroshio-Oyashio Extension (T. Qu et al., Subduction of the North Pacific mode waters in a global high-resolution GCM, submitted to *Journal of Physical Oceanography*, 2001). In addition to this effect of eddy momentum transport, the mechanisms for winter mixed layer depth distribution in the northwestern North Pacific, on which these western mode waters are dependent, are still poorly understood.

Acknowledgments. We thank A. Kubokawa and T. Suga for helpful discussions. The computations were performed at Hokkaido University Computing Center, with partial support from University of Tokyo's Center for Climate System Research. This is the IPRC contribution and SOEST contribution. The IPRC is partially supported by the Frontier Research System for Global Change. The figures are produced by the GFD-DENNOU library and the GrADS.

References

Bingham, F., Formation and spreading of Subtropical Mode Water in the North Pacific, *J. Geophys. Res*., *97*, 11,177–11,189, 1992.

Cox, M. D., Isopycnal diffusion in a *z*-coordinate ocean model, *Ocean Modell*., *74*, pp. 1–5, Hooke Inst., Oxford Univ., Oxford, Engl., 1987.

Gill, A. E., *Atmosphere-Ocean Dynamics*, 602 pp., Academic, San Diego, Calif., 1982.

Haney, R. L., Surface thermal boundary condition for ocean circulation models, *J. Phys. Oceanogr*., *4*, 241–248, 1971.

Hautala, S., and D. Roemmich, Subtropical Mode Water in the northeast Pacific Basin, *J. Geophys. Res*., *103*, 13,055–13,066, 1998.

Held, I. M., Stationary and quasi-stationary eddies in the extratropical troposphere: Theory, in *Large-Scale Dynamical Processes in the Atmosphere*, edited by B. J. Hoskins and R. Pearce, pp. 127–168, Academic, San Diego, Calif., 1983.

Huang, R. X., and J. Pedlosky, Climate variability induced by anomalous buoyancy forcing in a multilayer model of the ventilated thermocline, *J. Phys. Oceanogr*., *30*, 3009–3021, 2000.

Huang, R., and B. Qiu, Three-dimensional structure of the wind-driven circulation in the North Pacific, *J. Phys. Oceanogr*., *24*, 1608–1622, 1994.

Huffman, G. J., R. F. Adler, B. Rudolf, U. Schneider, and P. R. Keehn, Global precipitation estimates based on a technique for combining satellite-based estimates, rain gauge analysis and NWP model precipitation estimates, *J. Clim*., *8*, 1284–1295, 1995.

Inatsu, M., H. Mukougawa, and S.-P. Xie, Formation of subtropical westerly jet core in an idealized GCM without mountains, *Geophys. Res. Lett*., *27*, 529–532, 2000.

Inui, T., K. Takeuchi, and K. Hanawa, A numerical investigation of the subduction process in response to an abrupt intensification of westerlies, *J. Phys. Oceanogr*., *29*, 1993–2015, 1999.

Kalnay, E., et al., The NCEP/NCAR 40-year reanalysis project, *Bull. Am. Meteorol. Soc*., *77*, 437–471, 1996.

Kubokawa, A., Ventilated thermocline strongly affected by a deep mixed layer: A theory for subtropical countercurrent, *J. Phys. Oceanogr*., *29*, 1314–1333, 1999.

Ladd, C. A., and L. Thompson, Formation mechanisms for North Pacific central and eastern subtropical mode waters, *J. Phys. Oceanogr*., *30*, 868–887, 2000.

Levitus, S., and T. P. Boyer, *World Ocean Atlas 1994*, vol. 4, *Temperature*, *NOAA Atlas NESDIS*, vol. 4, 129 pp., Natl. Oceanic and Atmos. Admin., Silver Spring, Md., 1994.

Levitus, S., R. Burgett, and T. P. Boyer, *World Ocean Atlas 1994*, vol. 3, *Salinity*, *NOAA Atlas NESDIS*, vol. 3, 111 pp., Natl. Oceanic and Atmos. Admin., Silver Spring, Md., 1994.

Luyten, J. R., J. Pedlosky, and H. Stommel, The ventilated thermocline, *J. Phys. Oceanogr*., *13*, 292–309, 1983.

Masuzawa, J., Subtropical mode water, *Deep Sea Res. Oceanogr. Abstr*., *16*, 463–472, 1969.

McCartney, M., The subtropical recirculation of mode waters, *J. Mar. Res*., *40*, suppl., 427–464, 1982.

Nakamura, H., A pycnostad on bottom of the ventilated portion in the central subtropical circulation using an eddy-resolving quasi-geostrophic model, *J. Oceanogr*., *52*, 171–188, 1996.

Nonaka, M., and S.-P. Xie, Propagation of North Pacific interdecadal subsurface temperature anomalies in an ocean GCM, *Geophys. Res. Lett*., *27*, 3747–3750, 2000.

Pacanowski, R. C., K. W. Dixon, and A. Rosati, The GFDL Modular Ocean Model Users Guide, *GFDL Ocean Group Tech. Rep. 2*, Geophys. Fluid Dyn. Lab., Princeton, N. J., 1991.

Roemmich, D., and B. Cornuelle, The subtropical mode waters of the South Pacific Ocean, *J. Phys. Oceanogr*., *22*, 1178–1187, 1992.

Stommel, H., Determination of watermass properties of water pumped down from the Ekman layer to the geostrophic flow below, *Proc. Natl. Acad. Sci. U.S.A*., *76*, 3051–3055, 1979.

Suga, T., and K. Hanawa, Interannual variations of North Pacific Subtropical Mode Water in the 137°E section, *J. Phys. Oceanogr*., *19*, 1012–1017, 1995.

Suga, T., Y. Takei, and K. Hanawa, Thermostad distribution in the North Pacific subtropical gyre: The Central Mode Water and the Subtropical Mode Water, *J. Phys. Oceanogr*., *27*, 140–152, 1997.

Williams, R. G., The role of the mixed layer in setting the potential vorticity of the main thermocline, *J. Phys. Oceanogr*., *21*, 1803–1814, 1991.

Worthington, L. V., The 18°C water in the Sargasso Sea, *Deep Sea Res*., *5*, 297–305, 1959.

Xie, S.-P., T. Kunitani, A. Kubokawa, M. Nonaka, and S. Hosoda, Interdecadal thermocline variability in the North Pacific for 1958–1997: A GCM simulation, *J. Phys. Oceanogr*., *30*, 2798–2813, 2000.

S. Hosoda and K. Takeuchi, Institute of Low Temperature Science, Hokkaido University, Kita-ku, N19 W8, Sapporo, 060-0819, Japan. (hoso@lowtem.hokudai.ac.jp)

M. Nonaka and S.-P. Xie, International Pacific Research Center/SOEST, University of Hawaii at Manoa, 2525 Correa Road, Honolulu, HI 96822, USA.

(Received May 17, 2000; revised March 19, 2001;
accepted March 12, 2001.)